Atmospheric origins of variability in the South Atlantic meridional overturning circulation

Timothy Smith
Patrick Heimbach

July 3, 2018

The South Atlantic Ocean

- South Atlantic hosts complex water mass exchanges, review: [Garzoli and Matano, 2011]
- Warm waters enter from the Indian Ocean, cold waters from the Pacific
- Mixing and air-sea interactions transform these to surface waters which travel Northward as part of the Atlantic Meridional Overturning Circulation (AMOC)

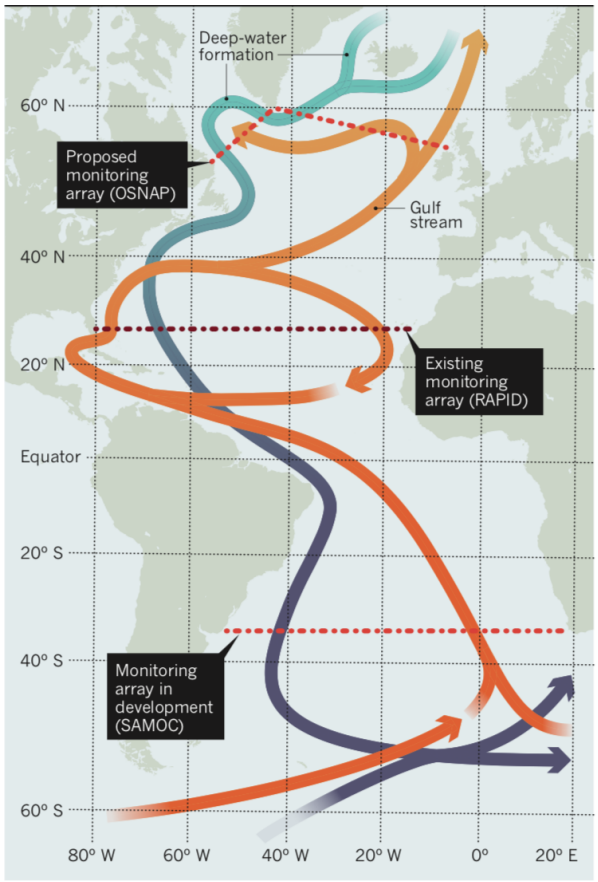

Figure: from [Schiermeier, 2013]

Variability in the SAMOC

- South Atlantic MOC Basin-wide Array (SAMBA) initiated to study impact on broader AMOC

  [Ansorge et al., 2014]

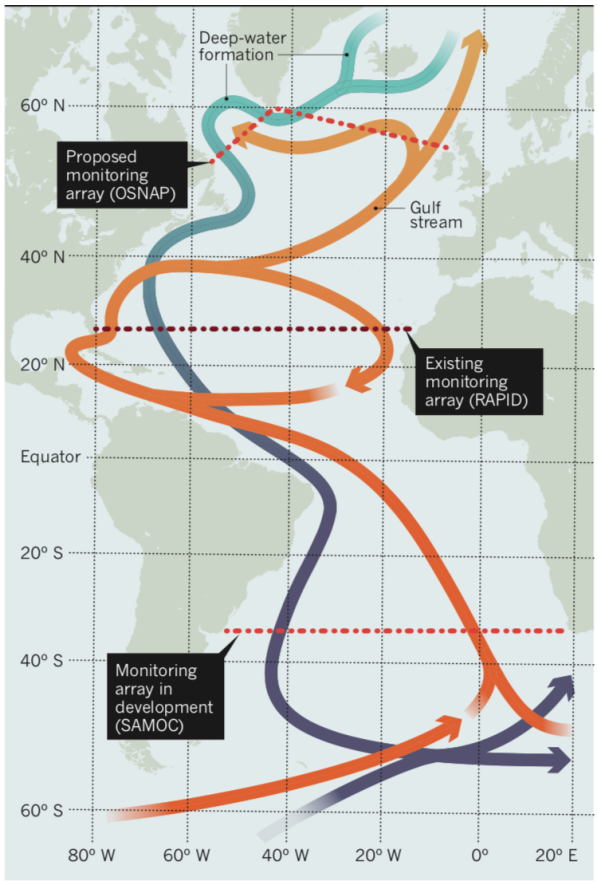

Figure: from [Schiermeier, 2013]

Variability in the SAMOC

- South Atlantic MOC Basin-wide Array (SAMBA) initiated to study impact on broader AMOC [Ansorge et al., 2014]
- What generates variability observed by SAMBA?

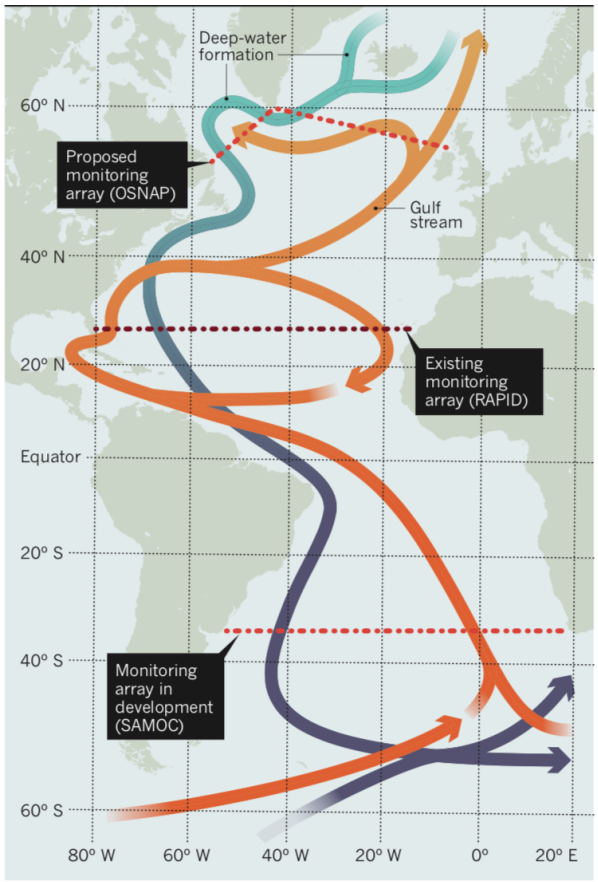

Figure: from [Schiermeier, 2013]

Variability in the SAMOC

- South Atlantic MOC Basin-wide Array (SAMBA) initiated to study impact on broader AMOC [Ansorge et al., 2014]
- What generates variability observed by SAMBA?

Goal

Attribute seasonal to interannual variability in the SAMOC to its geographical origins as atmospheric perturbations.

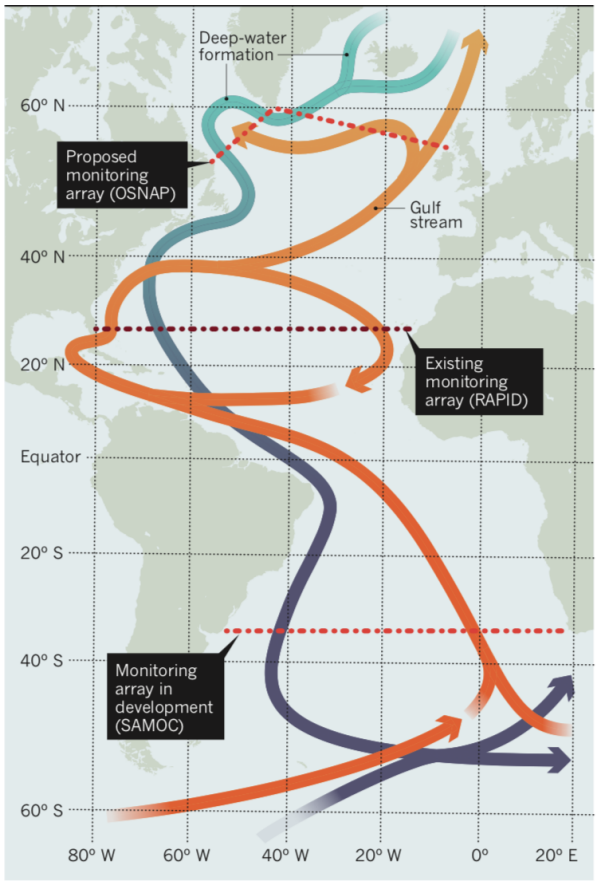

Figure: from [Schiermeier, 2013]

The Atlantic Meridional Overturning Circulation

- Overturning streamfunction at latitude y:

$$\psi_{MOC}(y,z,t) = -\int_{-H}^{z}\int_{x_W}^{x_E} v\, dx\, dz$$

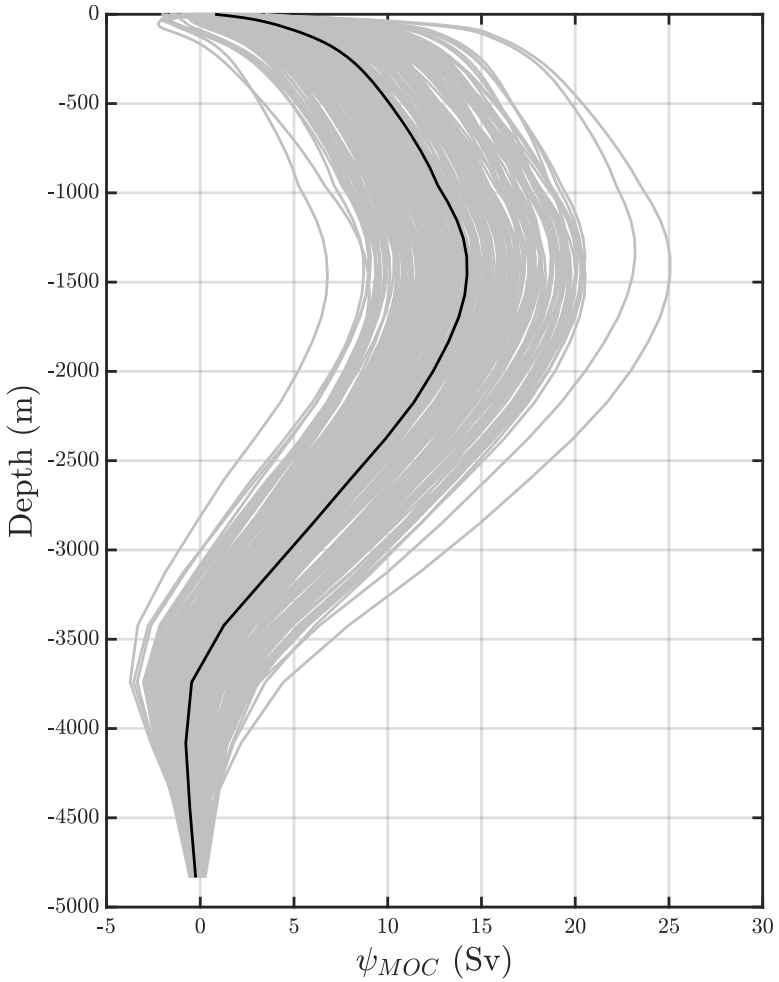

Figure: Monthly mean ψ_{MOC} at 34°S from ECCOv4r2 over 1992-2011.

The Atlantic Meridional Overturning Circulation

- Overturning streamfunction at latitude y:

$$\psi_{MOC}(y,z,t) = -\int_{-H}^{z}\int_{x_W}^{x_E} v\, dx\, dz$$

- AMOC is computed where ψ_{MOC} is maximized

$$AMOC(y,t) = \max_{z\in(-H,0)} \psi_{MOC}(y,z,t)$$

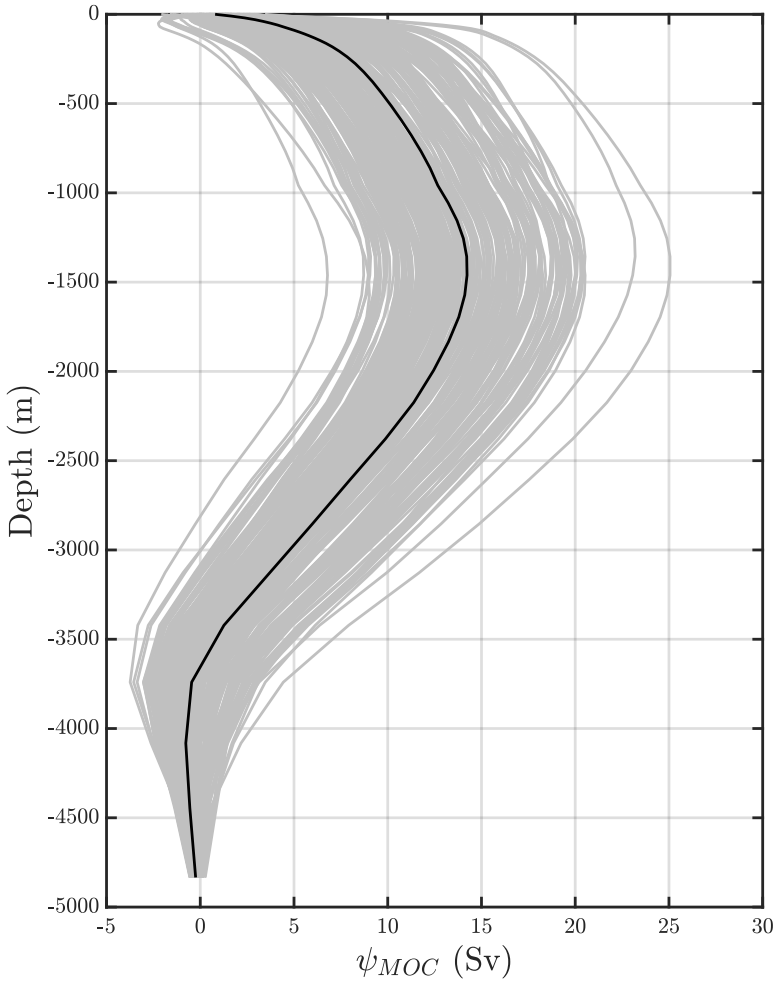

Figure: Monthly mean ψ_{MOC} at 34°S from ECCOv4r2 over 1992-2011.

The Atlantic Meridional Overturning Circulation

- Overturning streamfunction at latitude y:

$$\psi_{MOC}(y,z,t) = -\int_{-H}^{z}\int_{x_W}^{x_E} v\, dx\, dz$$

- AMOC is computed where ψ_{MOC} is maximized

$$AMOC(y,t) = \max_{z\in(-H,0)} \psi_{MOC}(y,z,t)$$

- A metric for global ocean circulation

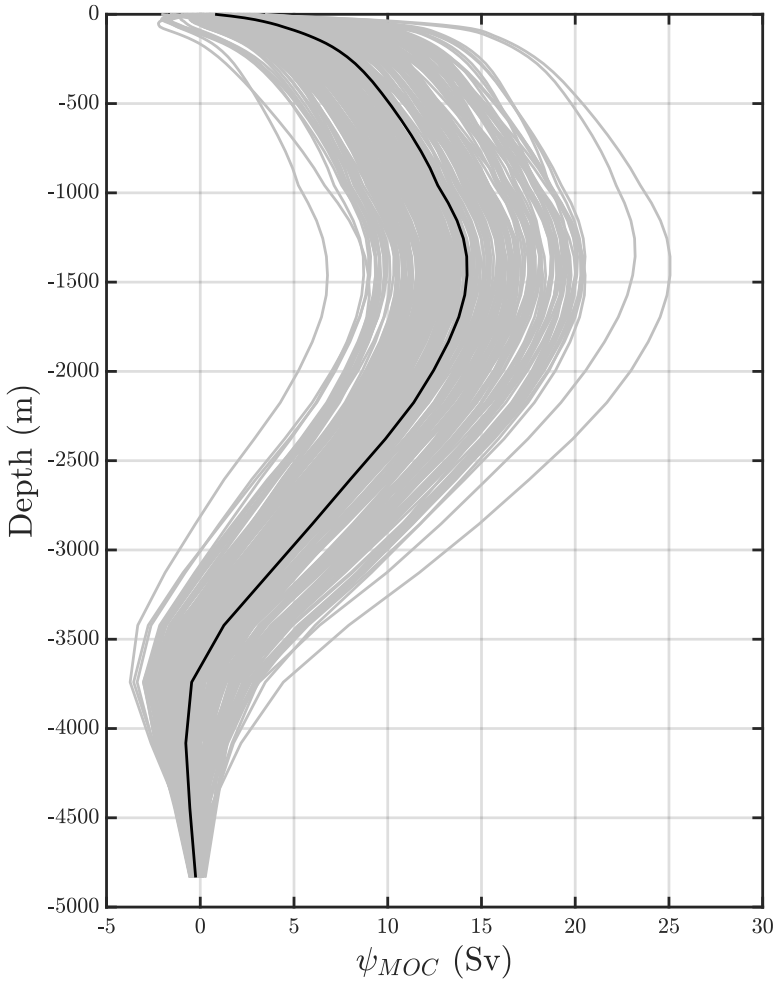

Figure: Monthly mean ψ_{MOC} at 34°S from ECCOv4r2 over 1992-2011.

Estimating the Circulation and Climate of the Ocean (ECCO)

Forward model:

- MITgcm: hydrostatic, Boussinesq equations from 1992-2011
- Finite volume discretization
- $\sim 1^\circ \times 1^\circ$ horizontal resolution, 50 vertical layers

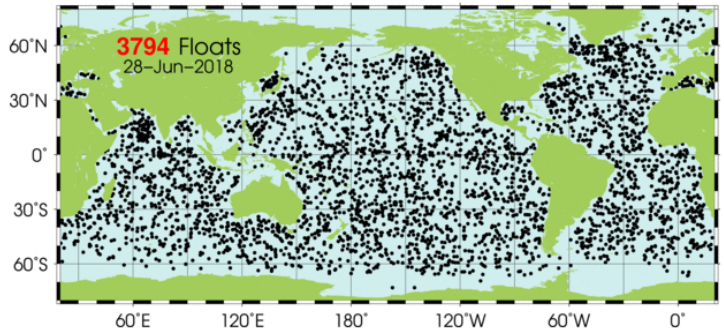

(a) June 28, 2018 Argo coverage `argo.ucsd.edu/About_Argo.html`

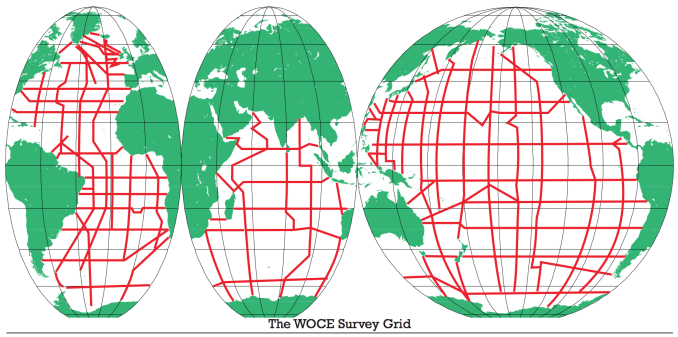

(b) from `nodc.noaa.gov/woce`

Estimating the Circulation and Climate of the Ocean (ECCO)

Forward model:

- MITgcm: hydrostatic, Boussinesq equations from 1992-2011
- Finite volume discretization
- $\sim 1^\circ \times 1^\circ$ horizontal resolution, 50 vertical layers

Inversion framework:

- Deterministic, nonlinear optimization (4D-Var) [Forget et al., 2015]
- Solve for uncertain
  - BCs: ERA Interim [Dee et al., 2011]
  - ICs: $(\mathbf{u}, \mathbf{v}, \theta, \mathbf{S})_0$
  - Parameters: $\kappa_{GM}, \kappa_{Redi}, \kappa_z$
- Adjoint based gradients computed via AD tool TAF [Giering et al., 2005]

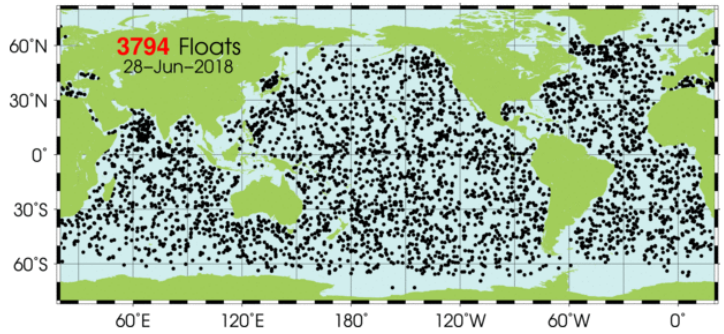

(a) June 28, 2018 Argo coverage `argo.ucsd.edu/About_Argo.html`

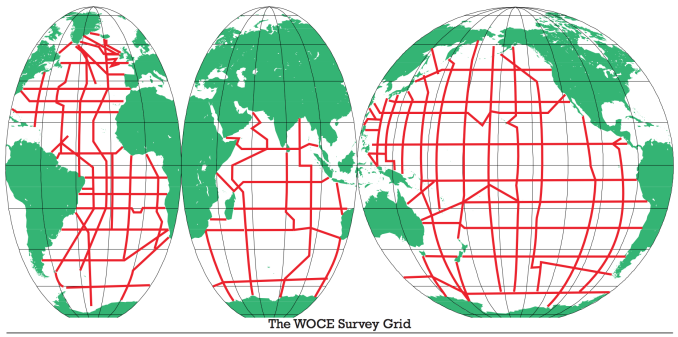

(b) from `nodc.noaa.gov/woce`

- Data include Argo, WOCE, GRACE, SSTs [Reynolds et al., 2002], etc.

Attribution of SAMOC variability

- Define $J^m := m^{th}$ monthly mean SAMOC at 34°S in final year of 1992-2011

Attribution of SAMOC variability

- Define $J^m := m^{th}$ monthly mean SAMOC at 34°S in final year of 1992-2011
- Consider linearized setting

$$J^m = \underbrace{J_0}_{20\ year\ mean} + \underbrace{\left\langle \left(\frac{\partial J^m}{\partial \mathbf{F}} \right)^T, \delta \mathbf{F} \right\rangle}_{\delta J^m}$$

Attribution of SAMOC variability

- Define $J^m := m^{th}$ monthly mean SAMOC at 34°S in final year of 1992-2011
- Consider linearized setting

$$J^m = \underbrace{J_0}_{20\ year\ mean} + \underbrace{\left\langle \left(\frac{\partial J^m}{\partial \mathbf{F}} \right)^T, \delta \mathbf{F} \right\rangle}_{\delta J^m}$$

- Two ingredients:
  - $\delta \mathbf{F} :=$ atmospheric forcing from ERA Interim with ECCOv4r2 adjustments [Dee et al., 2011, Forget et al., 2015]

Attribution of SAMOC variability

- Define $J^m := m^{th}$ monthly mean SAMOC at 34°S in final year of 1992-2011
- Consider linearized setting

$$J^m = \underbrace{J_0}_{\text{20 year mean}} + \underbrace{\left\langle \left(\frac{\partial J^m}{\partial \mathbf{F}} \right)^T, \delta \mathbf{F} \right\rangle}_{\delta J^m}$$

- Two ingredients:
  - $\delta \mathbf{F} :=$ atmospheric forcing from ERA Interim with ECCOv4r2 adjustments [Dee et al., 2011, Forget et al., 2015]
  - $\frac{\partial J^m}{\partial \mathbf{F}} :=$ sensitivity of SAMOC to atmospheric forcing, computed from ECCOv4r2 inverse modeling framework [Forget et al., 2015]

Reconstruction of SAMOC variability from a single point

How do zonal wind anomalies at one point during 1992 influence the January, 1993 SAMOC?

$$\delta J_{Rec}(t = \text{Jan, } 1993) = \int_{t-1\text{ yr}}^{t} \frac{\partial J^{m=1}}{\partial \tau_x}(x, y, s - t)\, \delta\tau_x(x, y, s)\, ds$$

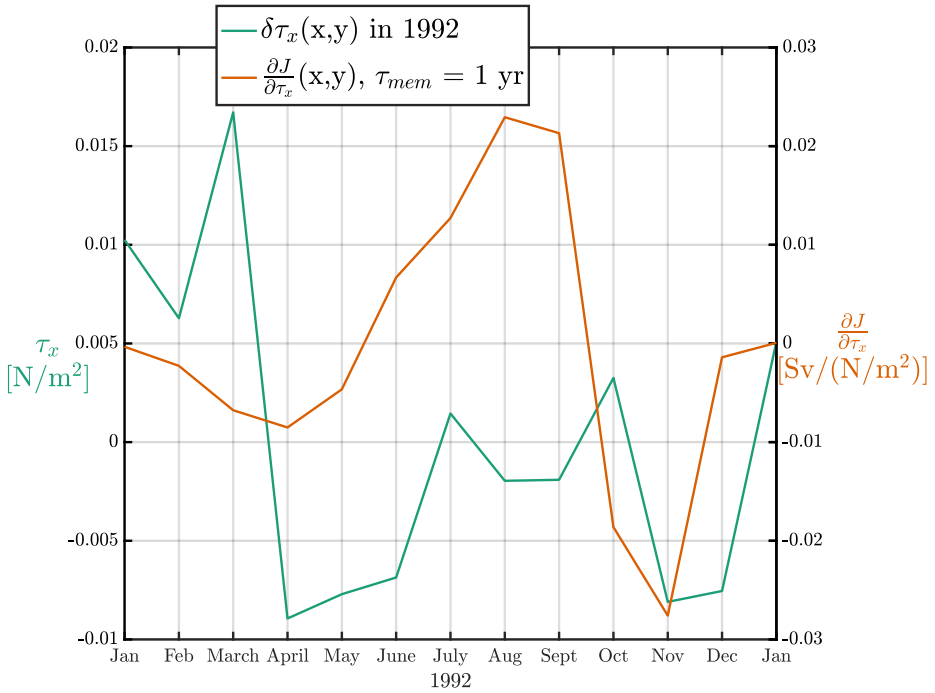

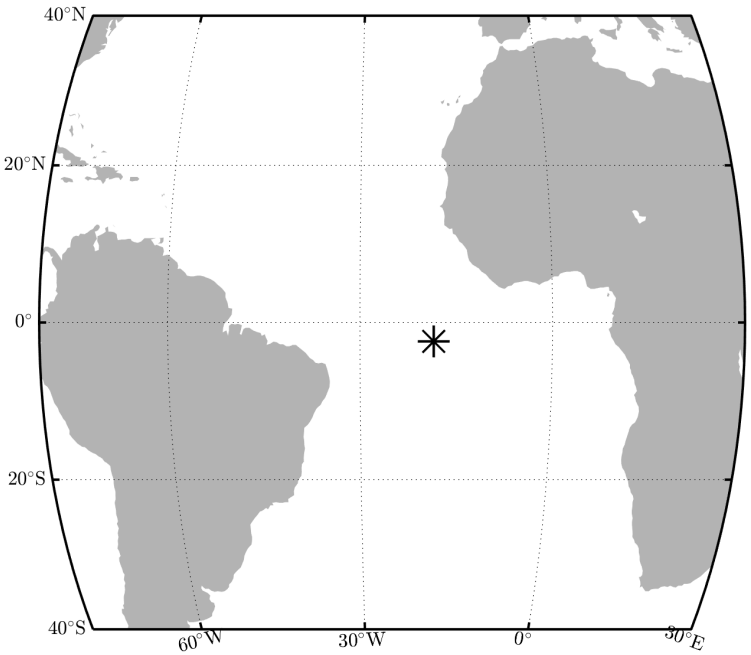

Reconstruction of SAMOC variability from a single point

How do zonal wind anomalies at one point during 1992 influence the January, 1993 SAMOC?

$$\delta J_{Rec}(t = \text{Jan, } 1993) = \int_{t-1\text{ yr}}^{t} \frac{\partial J^{m=1}}{\partial \tau_x}(x, y, s - t)\, \delta\tau_x(x, y, s)\, ds$$

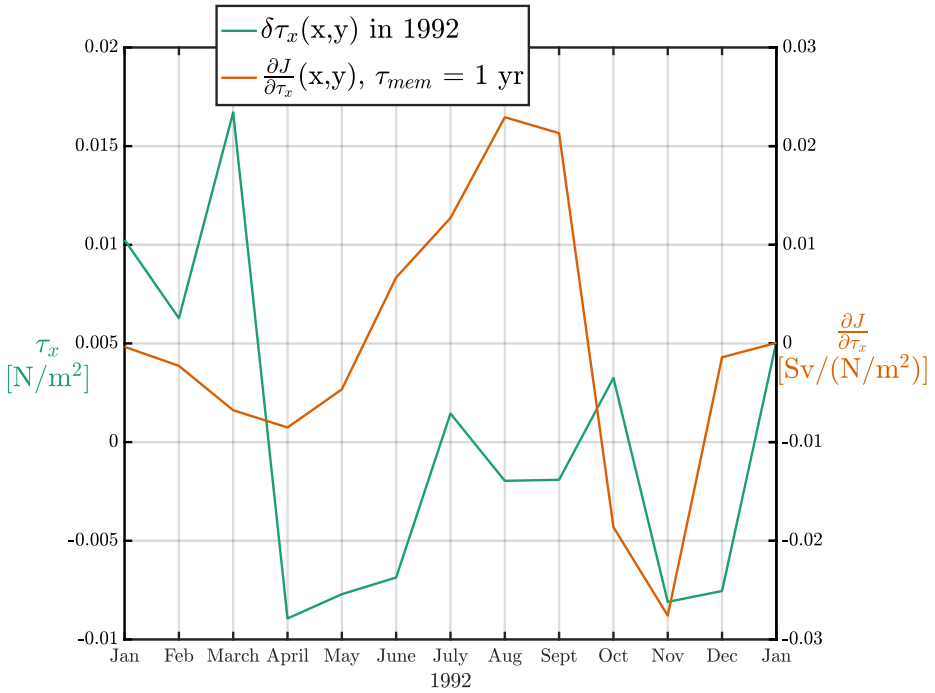

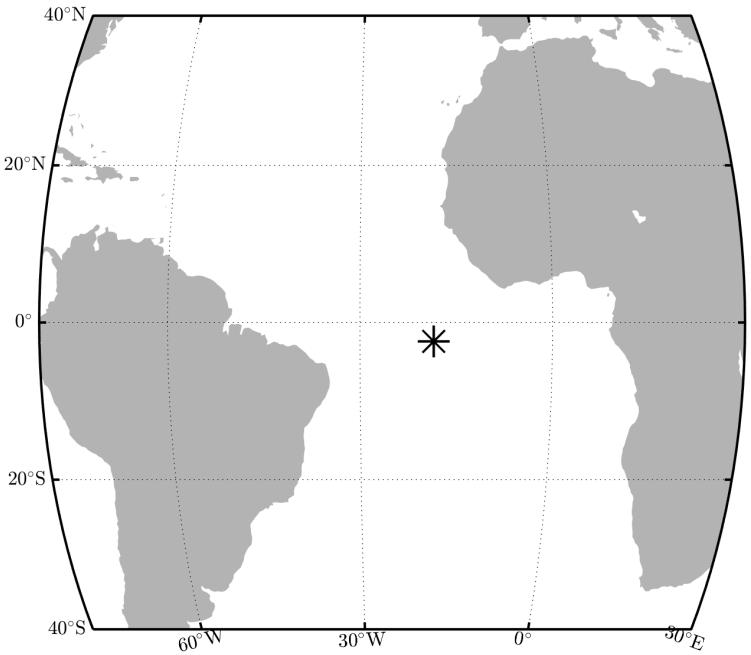

... not much, $\sim \mathcal{O}(10^{-5})$ Sv

Reconstruction of the SAMOC

$$\delta J_{Rec}(t) = \sum_k \delta J_k(t)$$
$$= \sum_k \int_{t-\tau_{mem}}^{t} \int_x \int_y \frac{\partial J^m}{\partial F_k}(x, y, s-t)\, \delta F_k(x, y, s)\, dx\, dy\, ds$$

- k indexes $\{$wind stress, long/short wave radiation, air temperature, humidity, precipitation, continental runoff$\}$
- τ_{mem} is the lead time, or SAMOC memory, max 19 years

Reconstruction of the SAMOC

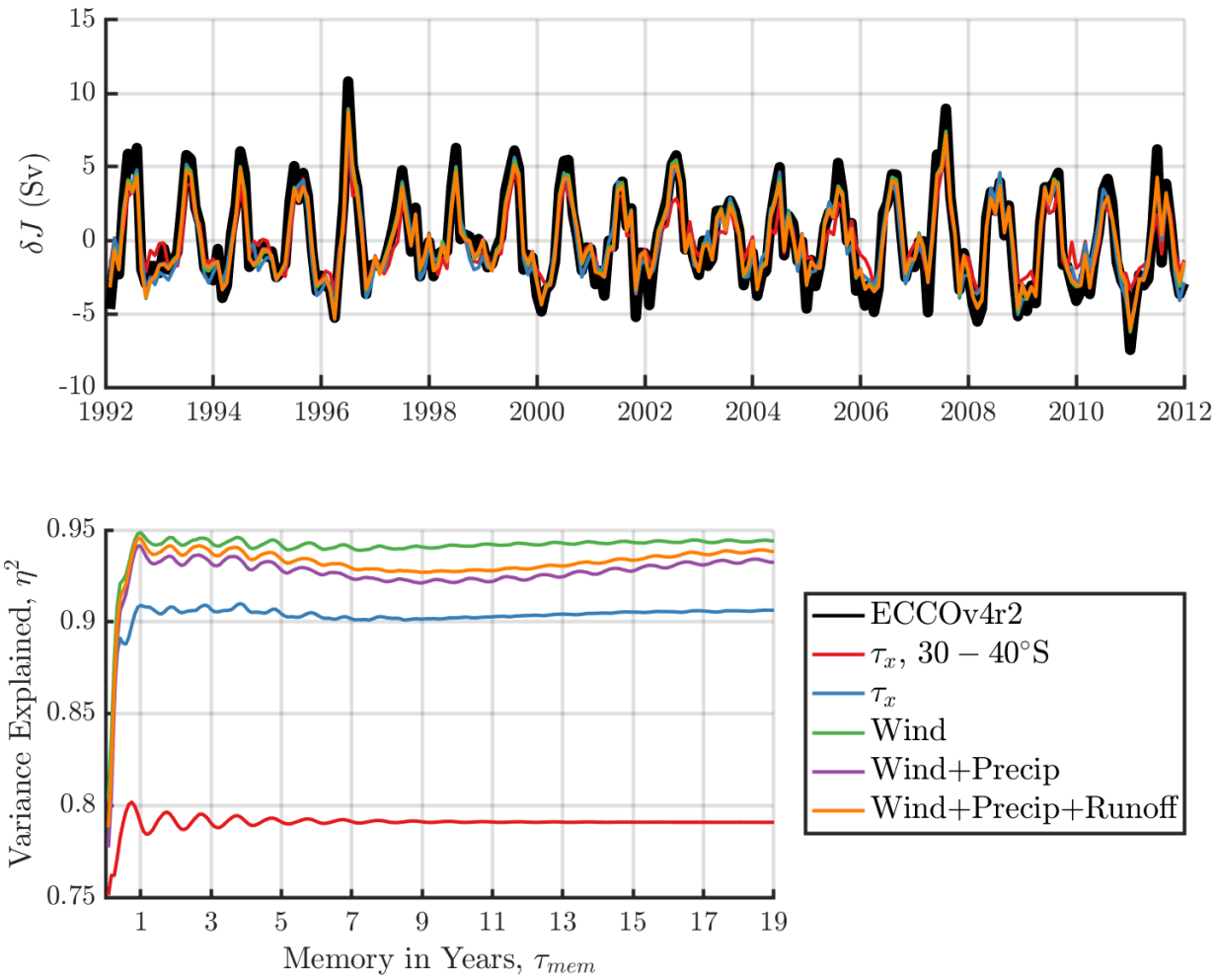

Figure: SAMOC at 34°S diagnosed from ECCOv4r2 (black) and various reconstructions. Lead time is 19 years.

Reconstruction of seasonal variability

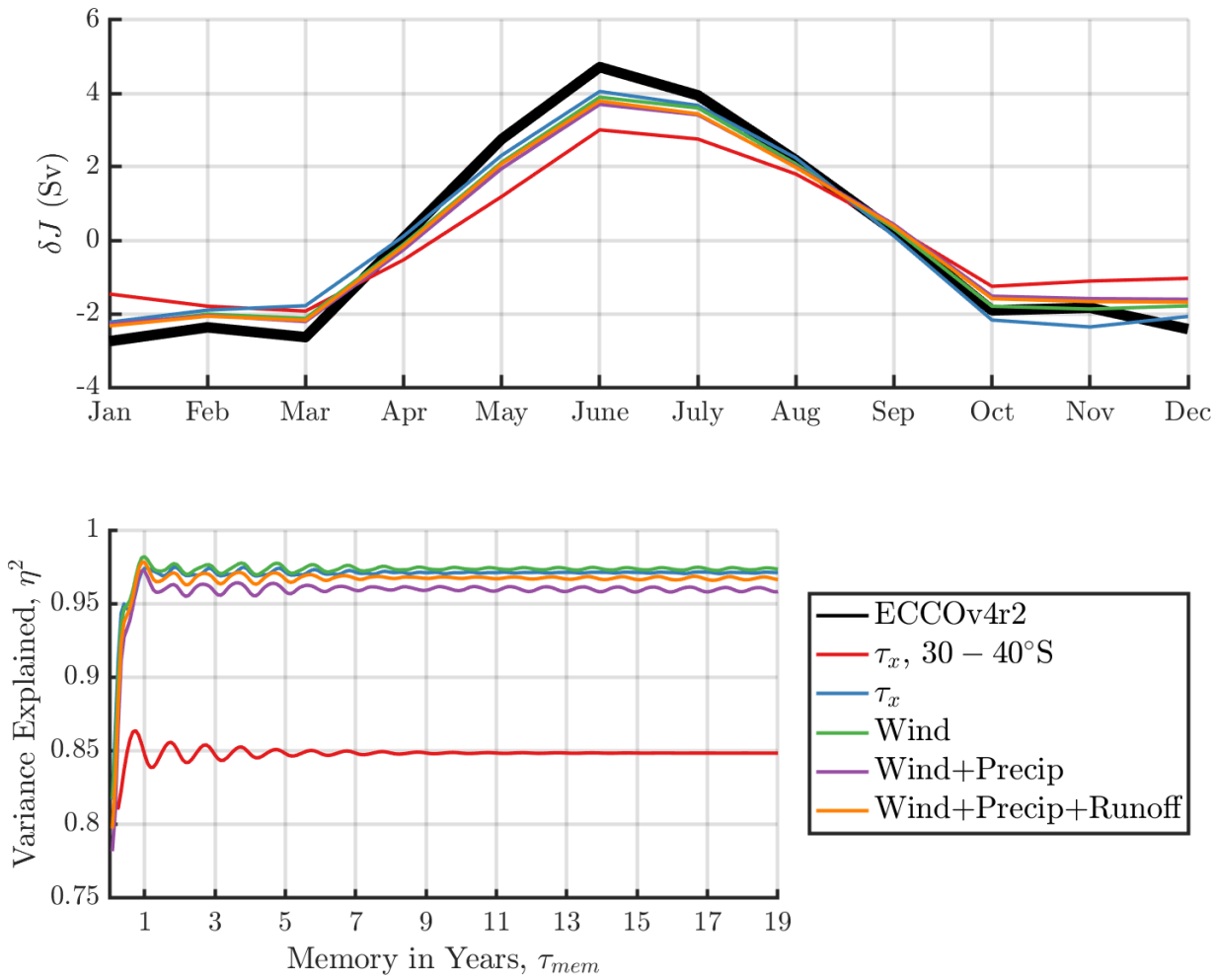

Figure: Reconstructed SAMOC seasonal variability compared to ECCOv4r2 output

Zonal wind seasonal cycle

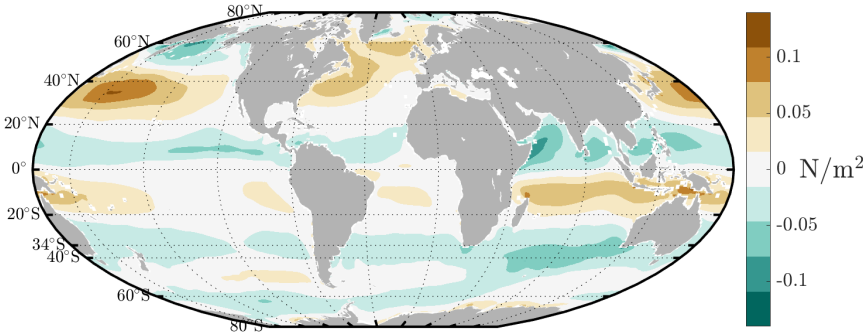

$\delta\tau_x$ Climatology
DJF Avg.

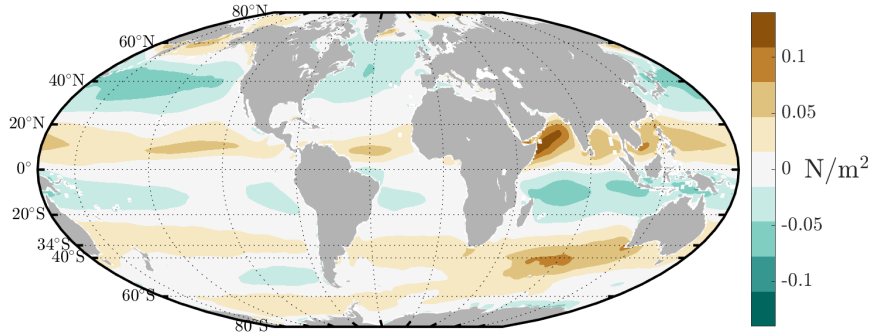

$\delta\tau_x$ Climatology
JJA Avg.

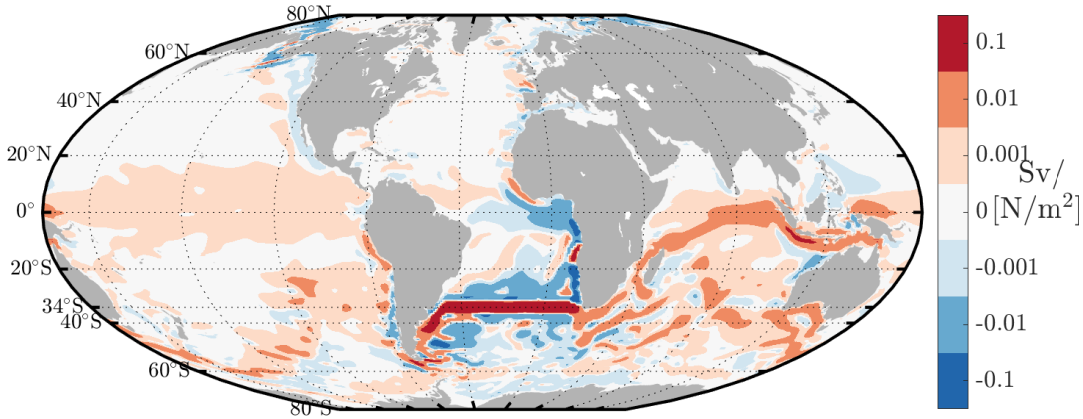

$\frac{\partial J}{\partial \tau_x}$, $\tau_{mem} = 1$ months

Attribution of the seasonal cycle

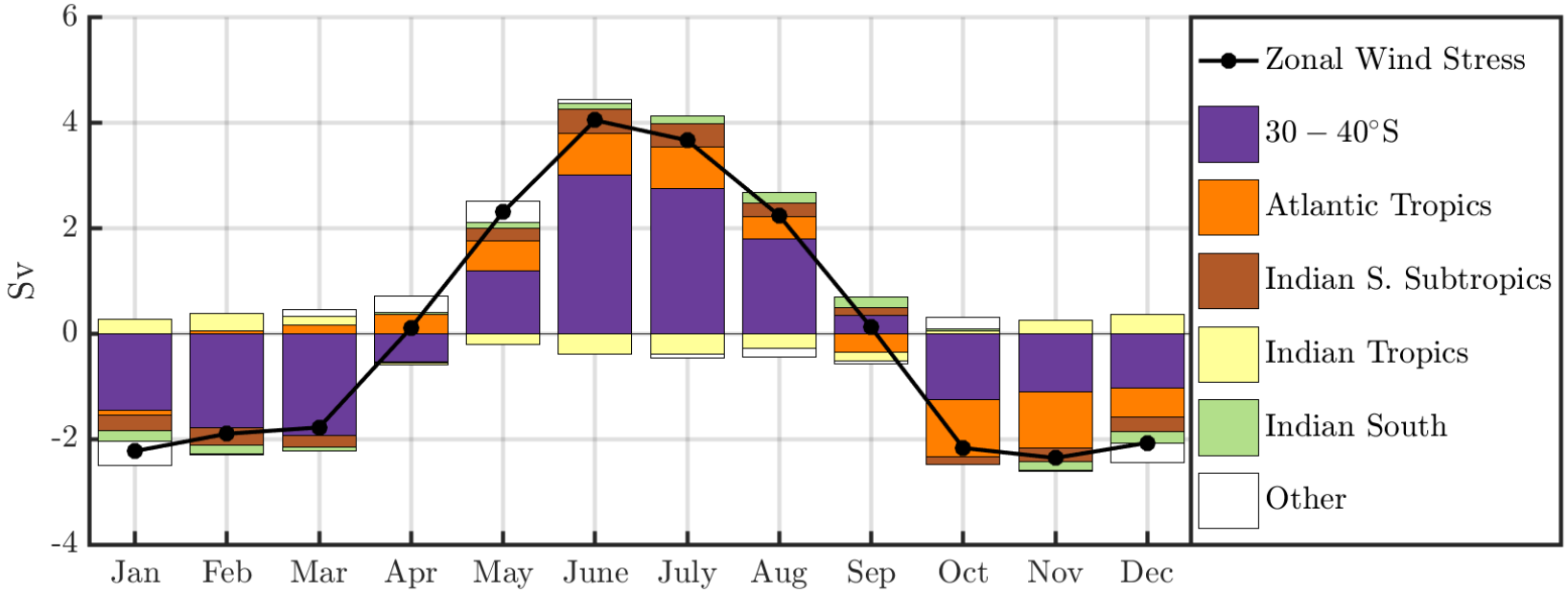

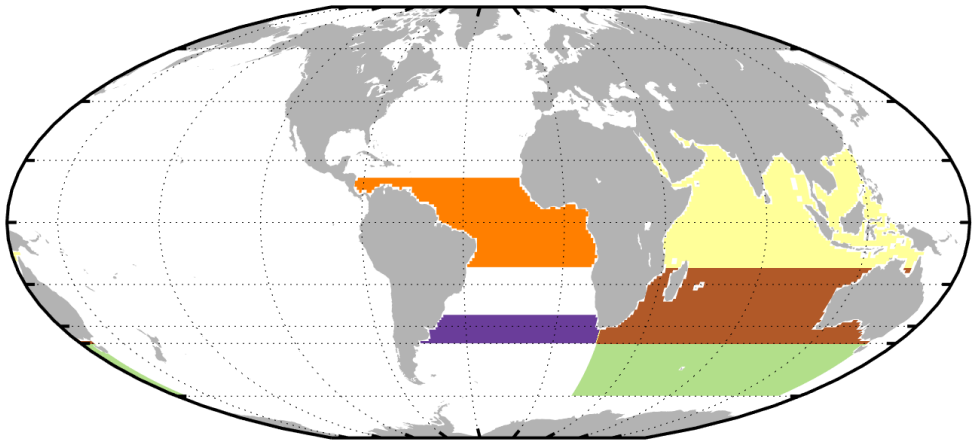

Attribution of interannual variability to zonal wind stress

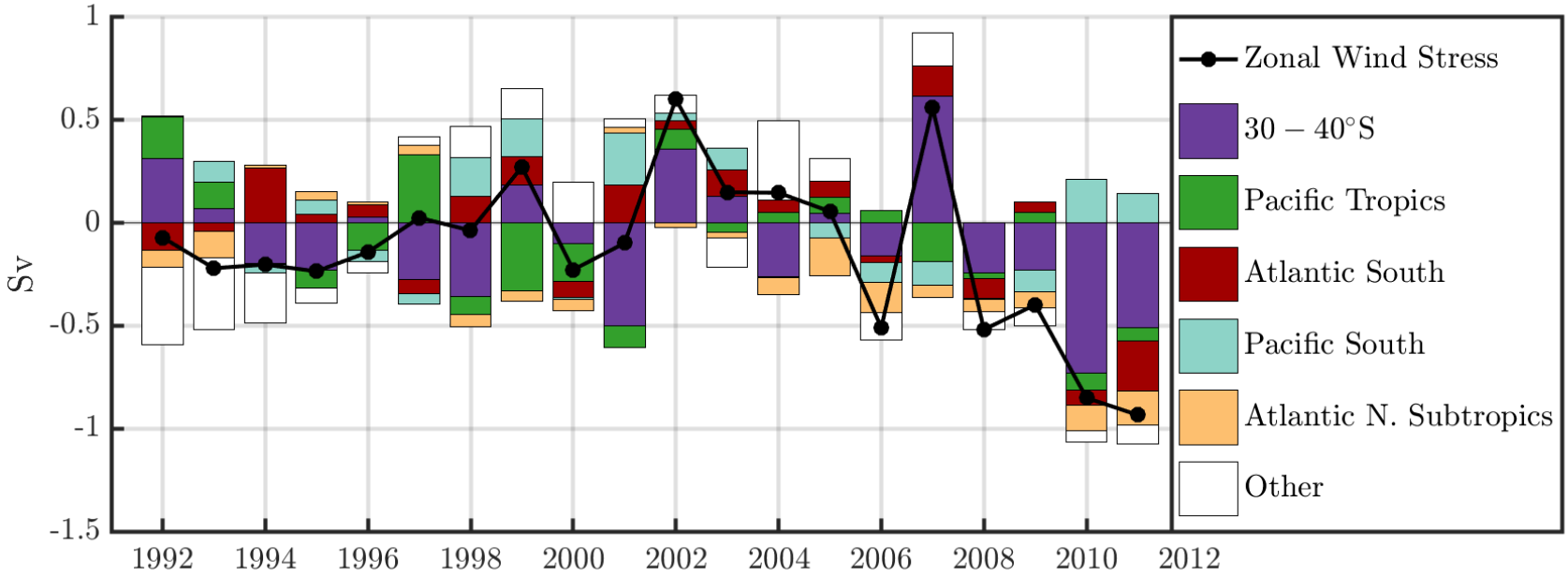

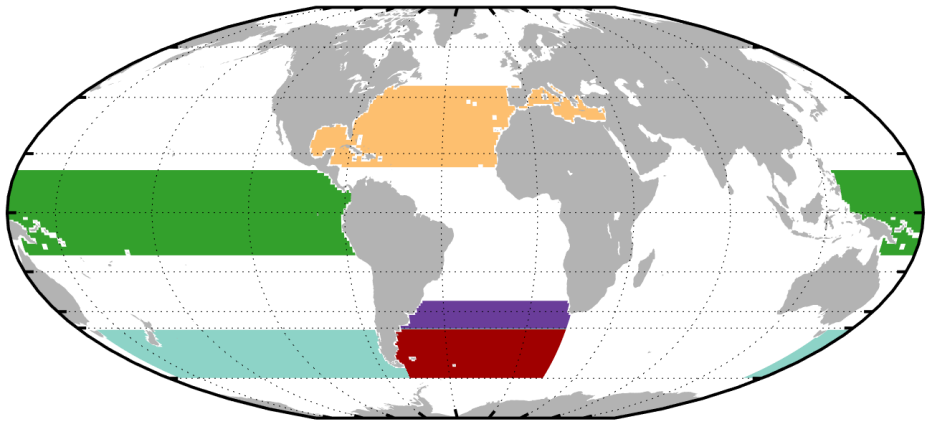

Variability attributed to ENSO

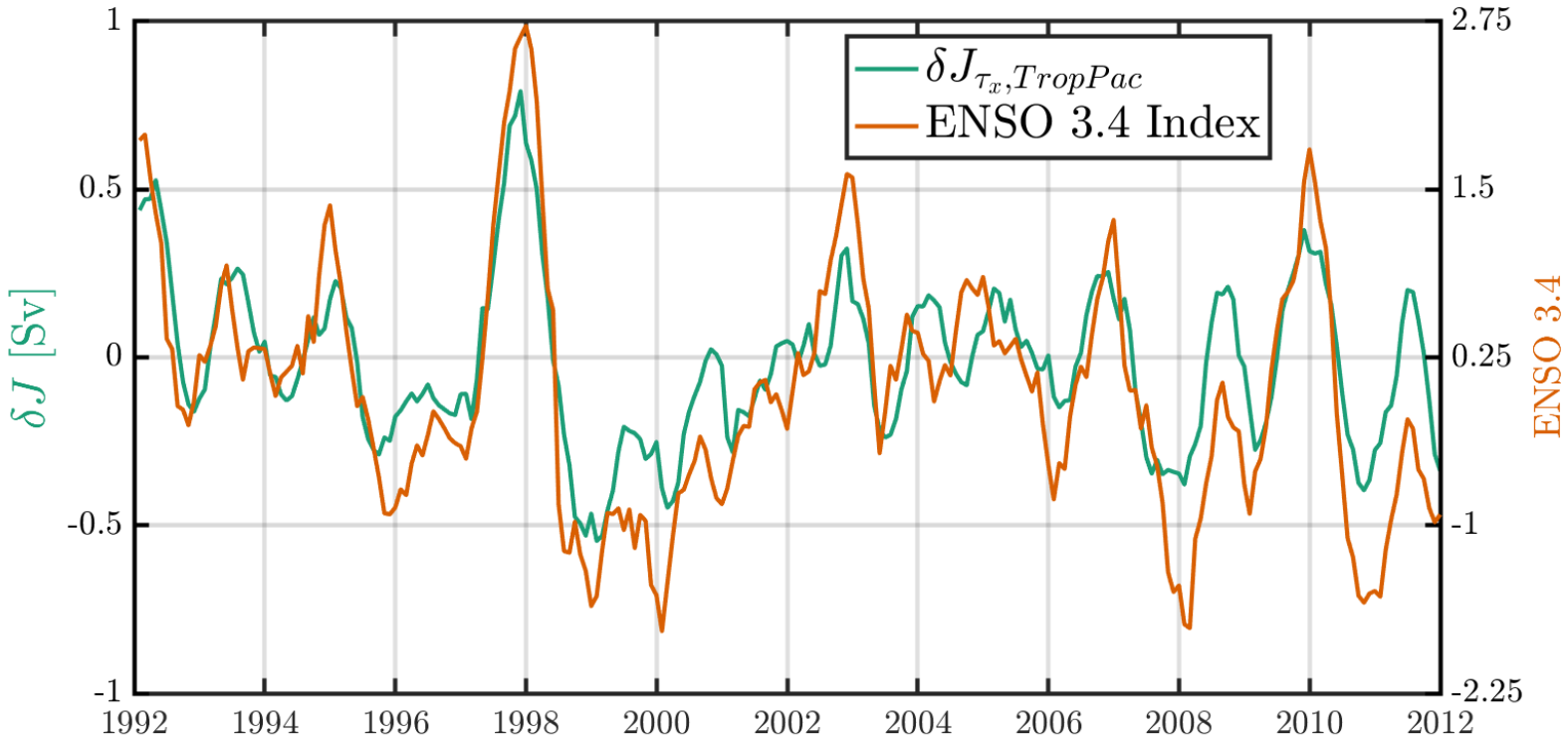

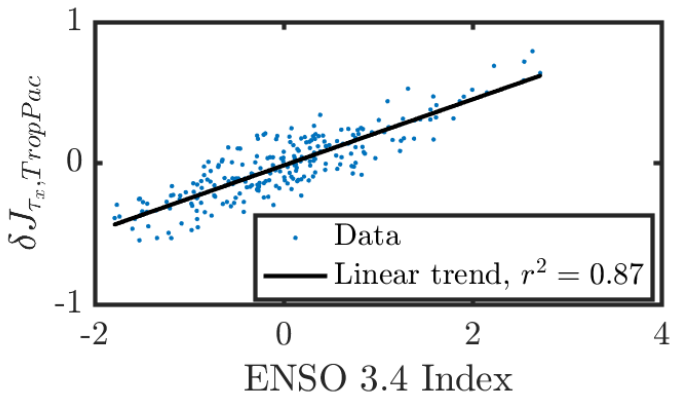

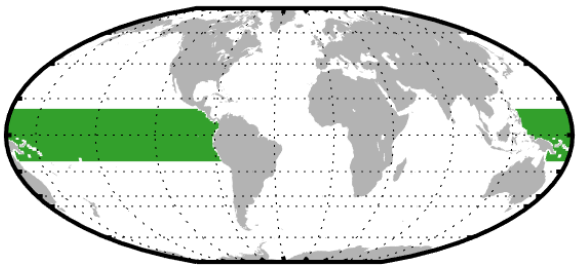

Conclusions

- Monthly AMOC variability well explained by linearized dynamics propagating atmospheric perturbations to 34°S

Conclusions

- Monthly AMOC variability well explained by linearized dynamics propagating atmospheric perturbations to 34°S
- Zonal wind stress, particularly from local forcing through Ekman dynamics, dominates the seasonal cycle

Conclusions

- Monthly AMOC variability well explained by linearized dynamics propagating atmospheric perturbations to 34°S
- Zonal wind stress, particularly from local forcing through Ekman dynamics, dominates the seasonal cycle
- Interannual variability shows complex dependence on remote forcing

Conclusions

- Monthly AMOC variability well explained by linearized dynamics propagating atmospheric perturbations to 34°S
- Zonal wind stress, particularly from local forcing through Ekman dynamics, dominates the seasonal cycle
- Interannual variability shows complex dependence on remote forcing
- The imprint of El Niño & La Niña is visible on the SAMOC, which can balance the impact of local forcing

Conclusions

- Monthly AMOC variability well explained by linearized dynamics propagating atmospheric perturbations to 34°S
- Zonal wind stress, particularly from local forcing through Ekman dynamics, dominates the seasonal cycle
- Interannual variability shows complex dependence on remote forcing
- The imprint of El Niño & La Niña is visible on the SAMOC, which can balance the impact of local forcing
- This relationship is shown through the model adjoint

References I

Ansorge, I. J., Baringer, M. O., Campos, E. J. D., Dong, S., Fine, R. A., Garzoli, S. L., Goni, G., Meinen, C. S., Perez, R. C., Piola, A. R., Roberts, M. J., Speich, S., Sprintall, J., Terre, T., and Van den Berg, M. A. (2014).
Basin-wide oceanographic array bridges the south atlantic.
Eos, Transactions American Geophysical Union, 95(6):53–54.

Dee, D. P., Uppala, S. M., Simmons, A. J., Berrisford, P., Poli, P., Kobayashi, S., Andrae, U., Balmaseda, M. A., Balsamo, G., Bauer, P., Bechtold, P., Beljaars, A. C. M., van de Berg, L., Bidlot, J., Bormann, N., Delsol, C., Dragani, R., Fuentes, M., Geer, A. J., Haimberger, L., Healy, S. B., Hersbach, H., Hlm, E. V., Isaksen, L., Kllberg, P., Khler, M., Matricardi, M., McNally, A. P., Monge-Sanz, B. M., Morcrette, J.-J., Park, B.-K., Peubey, C., de Rosnay, P., Tavolato, C., Thpaut, J.-N., and Vitart, F. (2011).

References II

The era-interim reanalysis: configuration and performance of the data assimilation system.
Quarterly Journal of the Royal Meteorological Society, 137(656):553–597.

Dong, S., Baringer, M. O., Goni, G. J., Meinen, C. S., and Garzoli, S. L. (2014).
Seasonal variations in the south atlantic meridional overturning circulation from observations and numerical models.
Geophysical Research Letters, 41(13):4611–4618. 2014GL060428.

References III


Forget, G., Campin, J.-M., Heimbach, P., Hill, C. N., Ponte, R. M., and Wunsch, C. (2015).
ECCO version 4: an integrated framework for non-linear inverse modeling and global ocean state estimation.
Geoscientific Model Development, 8(10):3071–3104.


Garzoli, S. L. and Matano, R. (2011).
The south atlantic and the atlantic meridional overturning circulation.
Deep Sea Research Part II: Topical Studies in Oceanography, 58(1718):1837 – 1847.
Climate and the Atlantic Meridional Overturning Circulation.


Giering, R., Kaminski, T., and Slawig, T. (2005).
Generating efficient derivative code with taf: Adjoint and tangent linear euler flow around an airfoil.
Future Generation Computer Systems, 21(8):1345 – 1355.

References IV

Reynolds, R. W., Rayner, N. A., Smith, T. M., Stokes, D. C., and Wang, W. (2002).
An improved in situ and satellite sst analysis for climate.
Journal of Climate, 15(13):1609–1625.

Schiermeier, Q. (2013).
Oceans under surveillance.
Nature, 497:167–168.

Reconstruction of interannual variability

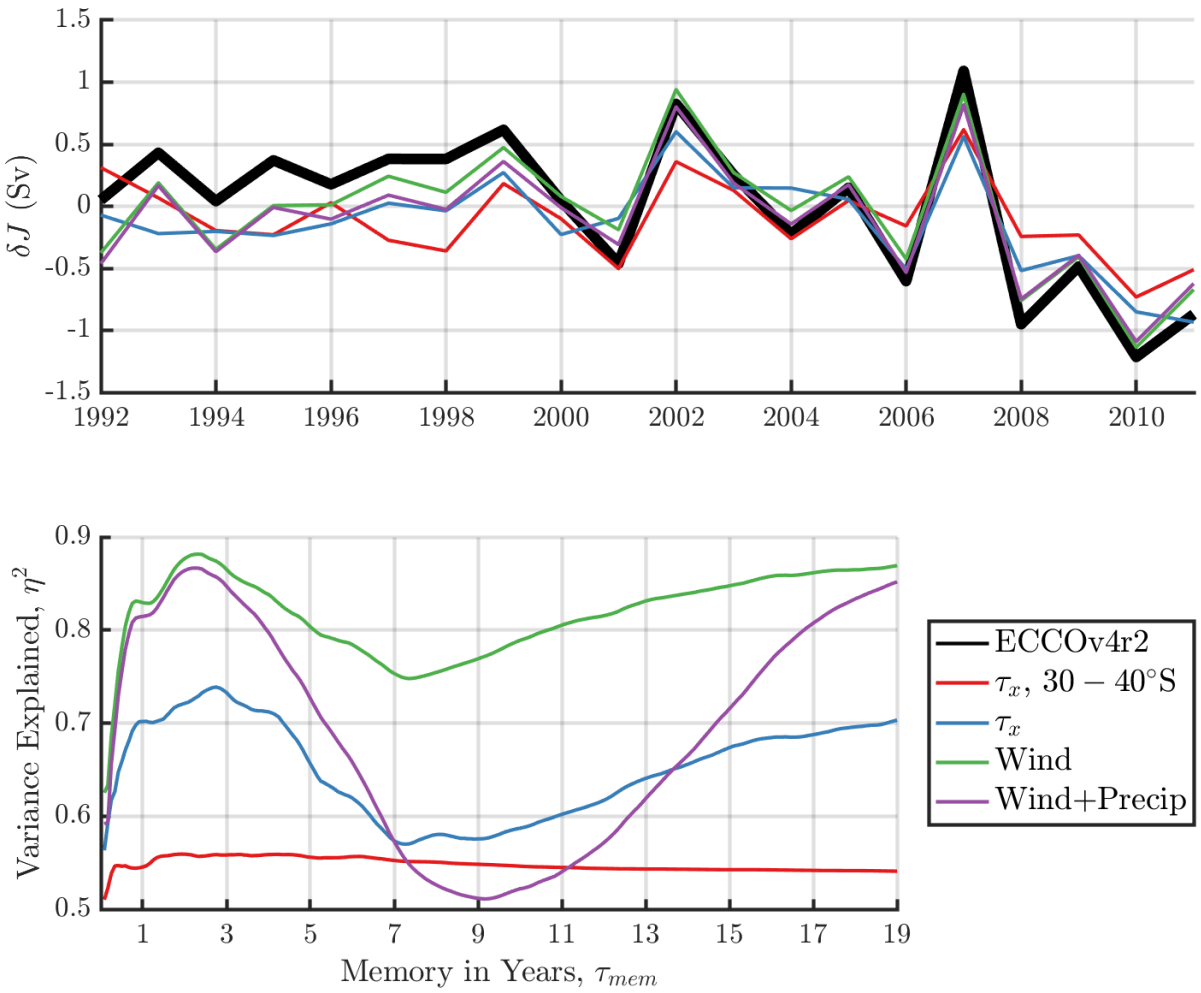

Figure: Reconstructed SAMOC interannual variability compared to ECCOv4r2 output

Comparison to Argo inferred SAMOC

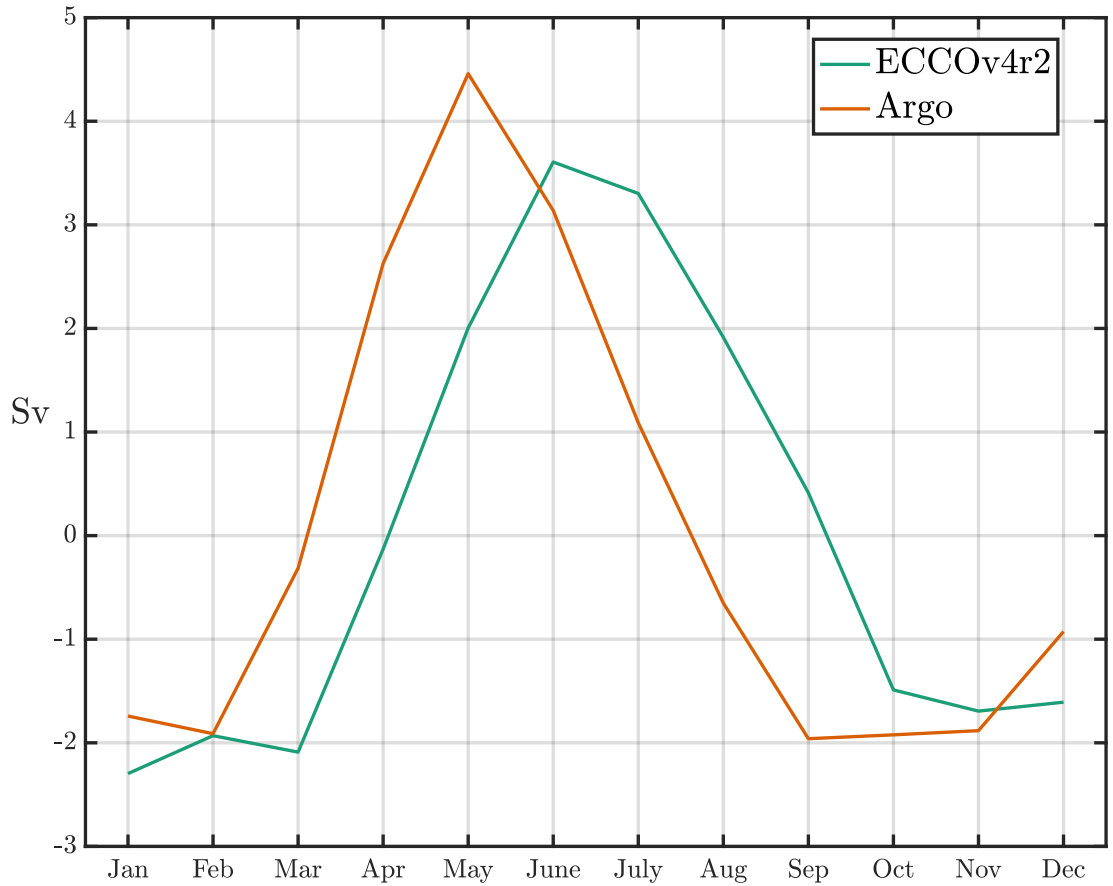

Figure: Comparison of SAMOC at 34°S (green) diagnosed from ECCOv4r2 and (orange) inferred from Argo profiles and Scatterometer Climatology of Ocean Winds (SCOW), from [Dong et al., 2014]

Attribution of interannual variability to heat flux

- Interannual reconstructions to air temperature, long & short wave radiation, and humidity diverge as $\tau_{mem} >\sim$ 5years
- Due to unphysically large sensitivities in N. Atl. Subpolar gyre & Weddell sea
- Results from parameterization of deep convection and brine rejection
- Further work to prove whether this is due to inexact adjoint formulation or nonlinearities

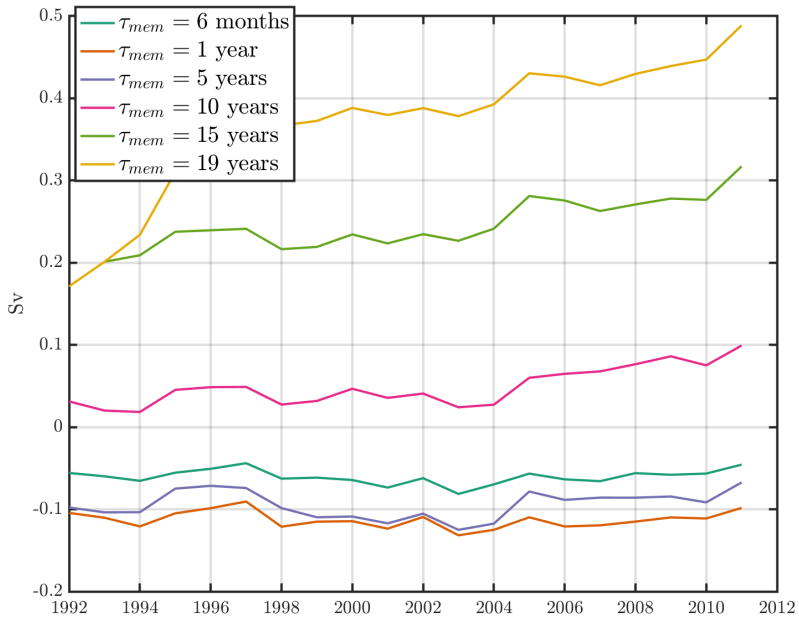

Figure: Reconstruction of interannual SAMOC variability due to shortwave radiation, shown as an example.